Journal of Engineering Science and Technology
Vol. 12, No. 2 (2017) 318 - 332

THE EFFECT OF V_2O_5 MELT INFILTRATION ON THE FAILURE OF THERMAL BARRIER COATINGS

ABBA ABDULHAMID ABUBAKAR*, SYED SOHAIL AKHTAR

Mechanical Engineering Department, King Fahd University of Petroleum & Minerals,
Box 1094, 31261, Dhahran, Saudi Arabia
*Corresponding Author: aabubakar@kfupm.edu.sa

Abstract

The use of low quality fuel in land based driven turbine in Saudi Arabia usually results in hot corrosion attack (Type 1) due to the penetration of V_2O_5 into the existing micro pores and cracks on the top coat of thermal barrier coatings (TBCs). As a result of dissolution-precipitation reaction, 4-5% volumetric expansion of the coating occurs due to the tetragonal-to-monoclinic (destabilization) transformation of Zirconia. In the current work, a Phase Field Model that estimates the kinetics of micro-structural evolution during the diffusional tetragonal-to-monoclinic phase transformation in the Melt Infiltrated Reaction Zone of the top coat at 900ºC is developed. The model is sequentially-coupled with constitutive model in order to determine the resulting stress field developed in the top coat. The results show that localized stresses are developed due to the Zirconia-destabilization transformation, and the stresses are found to be higher at the corners and curvatures formed by inter-lamella connection of the micro-pores and micro-cracks.

Keywords: Phase field model, Monoclinic phase, Tetragonal phase, Thermal barrier coating, Melt infiltrated reaction zone.

1. Introduction

Thermal Barrier Coatings (TBCs) are highly advanced coating materials that are usually applied to turbine blades operating at very high temperatures in order to improve their thermal and corrosion resistance [1]. TBC consists of four layers: the single-crystal base metal for structural support, metallic bond coat for corrosion/oxidation resistance, thermally grown oxide for oxidation resistance, and ceramic topcoat for thermal insulation [2]. Yttria-Stabilized Zirconia (YSZ) with 7 wt% to 8 wt% Yttrium Oxide (Y_2O_3) is the material most widely studied and

Nomenclatures

$D(t)$	Diffusion coefficient, m^2/s
F	Total free energy, J
f	Free energy density, J/m^3
L_1	Kinetic mobility, m^3/Js
l_o	Characteristic length, m
M_{vo}	Diffusion mobility, m^3/Js
T	Temperature, K
u	Displacement field, m
w_1	Height of double-well potential, J/m^3
X_p^{vo}	Equilibrium mole concentrations, moles
X_{VO}	Concentration of diffusing species, moles

Greek Symbols

α_1	Gradient energy coefficient, J/m
ε	Strain tensor
η_1	Order parameter/Phase field
υ	Global basis function
σ	Stress tensor, Pa

Abbreviations

FEM	Finite element method
MIRZ	Melt infiltrated reaction zone
m-phase	Monoclinic phase of zirconia
PDE	Partial differential equation
PFM	Phase field method
PRZ	Planar reaction zone
TBC	Thermal barrier coatings
t-phase	Tetragonal phase of zirconia
YSZ	Yttria stabilized zirconia

used for TBCs, because it provides the best performance at temperatures below 1,200°C. It basically contains the tetragonal phase of Zirconia which remains stable even after cooling to room temperature due to the stabilization by Y_2O_3 [3]. The porosity associated with YSZ has enabled it to have very low thermal conductivity which makes it a suitable material for TBC. Thus, it enables the blade to withstand very hot gas, erosion, corrosion, and damage due to foreign objects [1].

Some experiments [4] showed that as V_2O_5 reacts with the top coat, two sections or zones are created. First, a fine-grained section, the Planar Reaction Zone (PRZ), appears initially at the surface of the top coat and thickens/grows with increase in reaction time and temperature. The second section, the Melt Infiltrated Reaction Zone (MIRZ), is a dense infiltrated region with lamella structure and results from the reaction between the V_2O_5 that infiltrate through the pores of the coating and Y_2O_3 [5]. These zones are illustrated in Fig. 1. Different types of hot corrosion mechanisms that occur in TBCs were reviewed by Jones [6, 7]. Previous experiments showed that, the hot corrosion of the top coat occurs as a result of the reaction between the Vanadium impurities in fuel and ceramic top coat at high temperatures [4, 8]. These reactions result in the formation of a

molten salt (V_2O_5) which further reacts with the Yttrium ions in the top coat to leach a new phase, YVO_4 and cause the destabilization transformation of Zirconia. The overall effect of the evolution of these new phases is the volumetric expansion of the top coat by 4-5%, the development of localized stresses in the coating, propagation of cracks and subsequent failure of the TBC [9, 10], In fact, failure caused by hot corrosion can even precede failures due to sintering or the development of thermally grown oxide [10].

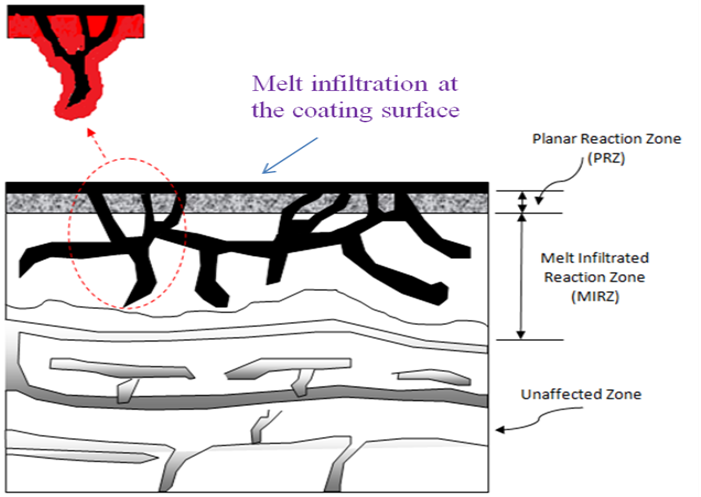

Fig. 1. Typical coating section showing planar reaction and melt infiltrated reaction zones.

In the current work, a Phase Field Model (PFM) is used to simulate the rate of destabilization-transformation of the Zirconia in the MIRZ due to the V_2O_5 hot corrosion. Prediction of the resulting stress field developed in the top coat is done by sequentially coupling PFM with material constitutive equations. Commercial Finite Element Package, COMSOL Multiphysics 4.3, is used for the computation.

2. Methodology

2.1. Phase field model

The phase field model (PFM) is a mathematical tool for solving interfacial problems. It treats interface as a surface of finite thickness using a variable called the phase field variable (or an order parameter), which describes the evolution of various phases in terms of space and time [11]. The phase field equations are usually developed based on thermodynamic principles and were first derived by Cahn and Hilliard [12] as well as Allen and Cahn [13]. The Cahn-Hilliard equations was derived based on principle of mass conservation and thus is suitably used for describing the evolution of conserved field variables such as mass or concentration. Conversely, the Allen-Cahn equation describes the evolution of non-conserved variable which is often used in tracking moving boundaries.

Many PFMs have been reported for a variety of solid-state phase transformation problems, such as corrosion kinetics of metals under dual oxidants

[14], nitriding process in steel [15], prediction of residual stresses in steel [16] and phase transformation of Low Carbon Steel [17], and precipitation of Al-Cu and Ti-Ni alloys [18] in the literatures. Although, PFM was developed for predicting the diffusionless tetragonal-to-monoclinic transformation of zirconia [19], we were the first to apply V_2O_5 diffusion-induced phase transformation of zirconia. Previous experimental work [4] showed that, the rate of destabilization transformation during the hot corrosion is not diffusionless but depends on the extent of exposure of the coating with the corrosive salt. So in our previous research [20], we developed a phase field model that predicts the stress fields developed during V_2O_5 hot corrosion of zirconia. The results show that the failure of TBC due to V_2O_5 hot corrosion may be due to grain boundary sliding and that the failure is dependent on the percentage and type of porosity.

In the following section, a PFM formulation for diffusional tetragonal-to-monoclinic phase transformation of zirconia in the MIRZ is described in detail. The solid state phase transformation is considered to be caused by the infiltration of chemical specie (V_2O_5) into top coat during the hot corrosion process.

2.2. Reaction in melt infiltrated reaction zone

As mentioned previously, the MIRZ forms as a result of the V_2O_5 infiltration through the microcracks and micropores that are common to air-plasma-sprayed TBCs. It was reported that, the infiltration starts immediately as the melt is in contact with the surface of the coating [4]. The time required for the melt to infiltrate through 300 μm depth of the coating at 750°C was found to be 30 minutes from experiments [4], and 3 seconds from Washburn Infiltration Model [21]. The discrepancy between experiments and the model is due to the various simplifying assumptions used by Washburn [21].

The failure of the coating in the current work is considered to occur at 900°C because it is the average operating temperature of turbine blades as well as the temperature at which highest degradation of the coating was reported for the TYPE-I hot corrosion process [22]. Thus, the corrosion reactions between the salt and the coating material is [8]:

$$ZrO_2(Y_2O_3) + V_2O_5 \rightarrow ZrO_2(\mathrm{m-phase}) + 2YVO_4 \quad (1)$$

However, estimation of the infiltration time at 900°C was not found in the open literature, and the Washburn model proves to be unreliable in predicting the infiltration time. For this reason, the infiltration time effect is neglected in the current work. And, the micropores/microcracks are assumed to be already filled with V_2O_5 when the transformation starts. The assumption is valid for the temperature and the typical crack section considered in the current work (shown in Figs. 2 and 3).

A typical crack-section of dimension 0.32×0.18 μm is taken for the analysis. The average crack/pore width or diameter is taken as 0.02 μm as determined experimentally in a previous work [4]. The melt is assumed to diffuse into the body of the coating in a direction that is normal to the reaction surface. The thickness of the crack-section is assumed to be far greater than the plane dimensions.

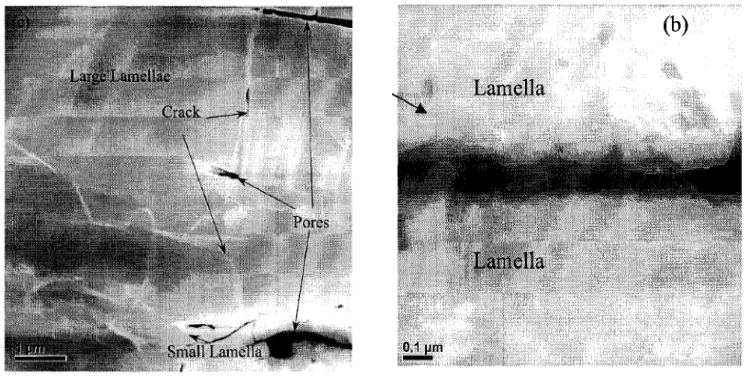

Fig. 2. SEM of MIRZ section showing cracks and pores in the top coat [23].

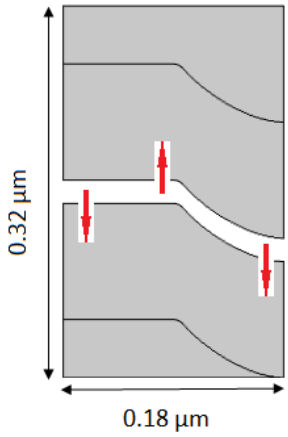

Fig. 3. Representative geometry for the model.

2.3. Model assumptions

Some major assumptions are made in formulating the PFM. They are outlined as follows:

- The transformation is considered to proceed in a direction normal to the reaction surface;
- Phase evolution due to vanadate is neglected;
- Infiltration time effect is neglected;
- Long-range elastic interaction is neglected, because chemical driving force is far greater than elastic strain energy;
- The diffusion coefficient of the melt is assumed to be constant in all phases;
- The tetragonal and monoclinic phases are assumed to be Isotropic and Inhomogeneous materials with phase-dependent elastic constants are used;
- Plain strain model is assumed, based on the selected coating cross-section.

2.4. Mathematical formulation

2.4.1. Field variables

Considering the phase evolution of the monoclinic phase, two phase-field variables are needed to represent the micro-structural distribution at a given time, t. One conserved phase-field variable for composition of molten salt and one non-conserved field variable for the evolution of the m-phase variable. The variable representing the evolution of the t-phase directly comes by the summation rule.

$\eta_1(x,y,t)$ is the non-conserved field variable (order parameter) which represents the evolution of the m-phase. It has a value of 1 for a pure m-phase and 0 for pure t-phase. X_{VO} is the conserved field variable representing the equilibrium mole concentration of V_2O_5. It has a value ranging from 0 to 0.56 moles corresponding to pure t-phase and m-phase respectively.

The third other variable is the displacement field variable through which the stress field can be computed based on the constitutive relation given in Eq. (6).

2.4.2. Governing equations

As described previously, the main equations describing the temporal and spatial evolution of the existing phases were developed by Cahn-Hilliard [12] for the concentration and Allen-Cahn/ Ginzburg-Laudau [13] for the order parameter. A constitutive model is needed to take care of the 4-5% volume expansion (swelling) of the top coat due to the phase transformation. It is given by the local force balance equation for deformable solid materials as given in Eq. (4).

Applying the Allen-Cahn and Cahn-Hilliard equations to the hot corrosion process result in the following PDE's [14]:

$$\frac{\partial \eta_1(x,y,t)}{\partial t} = -L_1\left(\frac{\partial f}{\partial \eta_1} - \alpha_1 \nabla^2 \eta_1\right) \tag{2}$$

$$\frac{\partial X_{VO}(x,y,t)}{\partial t} = \left[M_{VO}\nabla.\nabla\left(\frac{\partial f}{\partial X_{VO}}\right)\right] \tag{3}$$

$$-\nabla \cdot \sigma = 0 \tag{4}$$

where x and y are spatial coordinates, t is time, L_1 is the kinetic mobility, M_{VO} is the diffusion/atomic mobility of V_2O_5, σ is the Cauchy stress tensor.

Using Kim-Kim Suzuki model [24], the local free energy function/density of the two phase zone can be expressed as:

$$f(\eta_1, X_{VO}) = h(\eta_1) f_m({X_{m-z}}^{vo}, T) + [1 - h(\eta_1)] f_t({X_{t-z}}^{vo}, T) + w_1 g(\eta_1) \tag{5}$$

where w_1 is the height of double-well potential, $f_m({X_{m-z}}^{vo}, T)$ is the chemical free energy of the m-phase, $f_t({X_{t-z}}^{vo}, T)$ is the chemical free energy of the t-phase, $h(\eta_1) = -2{\eta_1}^3 + 3{\eta_1}^2$ is the type-II interpolation function and $g(\eta_1) = {\eta_1}^2(1-\eta_1)^2$ is the double-well potential. Note that ${X_{t\text{-}z}}^{vo}$ and ${X_{m\text{-}z}}^{vo}$ are the equilibrium mole compositions of the molten salt in the different phases which can be obtained from a thermodynamic database.

The increment in Cauchy stress tensor is usually given by,

$$d\sigma = C^e : d\varepsilon^e \tag{6}$$

where C^e is the elastic stiffness tensor, and ε^e is the elastic strain tensor.

By additive decomposition the incremental strain at any given time,

$$d\varepsilon^e = d\varepsilon - d\varepsilon^{SW} = 0.5((\nabla u)^T + \nabla u) - d\varepsilon^{SW} \tag{7}$$

where ε is the total strain tensor, ε^{SW} is the swelling strain tensor and u is the displacement field. The inelastic part is assumed to be dominated by the swelling strain and proceed according to the kinetics for the phase transformation.

2.4.3. Initial and boundary conditions

Initial conditions (at t=0) for the model are:

$$\eta_1(x, y, 0) = 0 \tag{8}$$

$$X_{VO}(x, y, 0) = 0 \tag{9}$$

For the stress analysis, natural initial condition on the displacement field is adopted.

Boundary conditions used for the phase field model (shown in Fig. 4) are:

$$\eta_1(0, y, t) = 1, \quad X_{VO}(0, y, t) = 0.56 \tag{10}$$

$$\eta_1(50, y, t) = 0, \quad X_{VO}(50, y, t) = 0 \tag{11}$$

$$\frac{\partial \eta_1}{\partial x} = 0 \quad \text{and} \quad \frac{\partial X_{VO}}{\partial x} = 0 \tag{12}$$

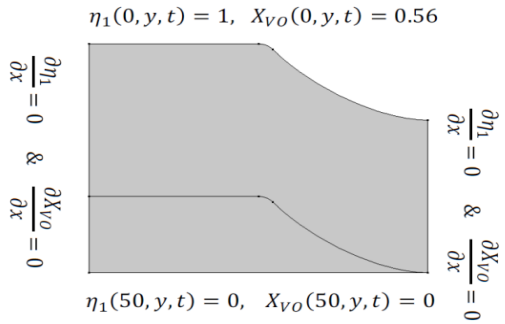

Fig. 4. PFM boundary conditions.

The boundary conditions signify that at all times, the surface of the crack cross section is exposed to 56 mol% of the diffusing specie resulting in the nucleation of the m-phase from the surface.

For the stress analysis, boundary conditions used are shown in Fig. 5. Symmetrical boundary condition is applied at the left boundary, roller supports are

applied at the bottom boundary, and the nodes at the right boundary are constrained to have same degree of freedoms in *x* direction (i.e., coupled boundary condition).

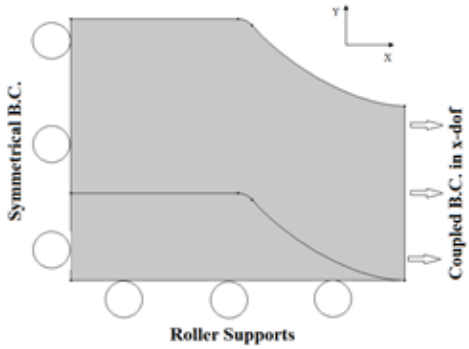

Fig. 5. Boundary conditions.

2.4.4. Normalization

Due to the fact that the dimensional parameters are at micro-scale, it is necessary to normalize the governing equations for the PFM with the following characteristic constants.

$$\bar{x} = \frac{x}{l_0}, \bar{f} = \frac{f}{\Delta f_{max}}, \bar{t} = \frac{M_{VO} \cdot \Delta f_{max} \cdot t}{(l_0)^2} \tag{13}$$

$$\bar{M}_{VO} = 1, \bar{L}_1 = \frac{L_1 (l_0)^2}{M_{VO}}, \bar{\alpha}_1 = \frac{\alpha_1}{(l_0)^2 \cdot \Delta f_{max}} \tag{14}$$

where l_0 is the characteristic length for grid scaling, Δf_{max} is a constant related thermodynamic property of the material.

2.5. Numerical implementation

For ease of computations, a mapped mesh was used to carry out the analysis and the time discretization is done using Backward Difference Approximation (BDA) of 1st-5th order. The domain has a total number of 20480 quadrilateral elements and 550,067 degree of freedoms. In order to confirm the accuracy of the finite element results, convergence tests were carried out for both the phase transformation and the stress analysis. Time-independent test was also carried out and the solutions were found to converge for the 1000 time steps used.

2.6. Simulation parameters

The simulation parameters used are shown in Tables 1 and 2.

Table 1. Constitutive model parameters.

Parameter	Value	Source
Modulus of Elasticity of m-phase	21GPa	[25]
Modulus of Elasticicty of t-phase	40GPa	[26]
Poisson Ratio of m-phase	0.25	[25]
Poisson Ratio of t-phase	0.22	[26]

Table 2. PFM Simulation parameters.

Parameters	Value	Source
Pore melt composition(X_{VO})	56 mol% or 3wt% V_2O_5	[4]
Temperature (T)	900°C	
Equil. Conc. of V_2O_5 in YSZ(X_{t-z}^{vo})	0.2	[5]
Equil. Conc. of V_2O_5 in m-ZrO_2(X_{m-z}^{vo})	0.5	[5]
Diffusion Coefficient($D(T)$) of V_2O_5	$1.0 \times 10^{-10} m^2/s$	[27]
Chemical Driving Force	39.66×10^6 J/m^3	[19]
Kinetic Coefficient(L_1)	2 m^3/ J s	[19]
Thickness of Interface(l)	0.01 μm	
Gradient Energy Coefficient(α_1)	1×10^{-8} J/m	[19]
Characteristic Length (l_o)	1 μm	

3. Results and Discussions

3.1. Validation

In our previous work [20, 28], a PFM model was calibrated to predict the transformation-induced stresses developed during the hot corrosion failure of TBCs. The results show that high stresses developed in the PRZ lead to the nucleation and propagation of cracks along the splat grain boundaries that are common to air plasma-sprayed TBCs; thus resulting in the ultimate failure of the coatings. Furthermore, the model was used to investigate the effect of porosity in hot corroded TBCs [29]. It was shown that percentage porosity, pores shapes, and pores dispersion have a remarkable effect on the hot corrosion failure of TBCs.

Since the same reaction occurs in both the PRZ and MIRZ, the previously developed model is currently used for the analysing the stresses that are formed in the MIRZ. This will help in predicting the effect of melt infiltration in hot corroded TBCs. Due to the localized nature of the stresses and the high temperature of the process, experimental results of the stresses are not found in the open literature. Similarly, this is the first quantitative prediction of such failure stresses. However, the finite element results is also able to qualitatively prove that damage of hot corroded TBCs is contributed by melt infiltration through the micro-pores/lamellar present in air plasma-sprayed TBCs. For instance, Fig. 6 shows that lamellar structures in MIRZ are substantially damaged due to melt infiltration even before the complete failure of TBCs. The model gives a good insight as to why the rate of hot corrosion failure is higher than other modes of failures in TBCs.

3.2. Corrosion kinetics

The evolution of the monoclinic phase due to the V_2O_5 hot corrosion of Zirconia in the MIRZ was simulated using PFM. The transformation occurs due to the infiltration of the molten salt V_2O_5 into the open cracks/pores of the coating at 900°C. The transformation was prescribed to proceed in a direction normal to the reaction surface.

Figures 7 and 8 show the spatial evolution of the V_2O_5 concentration and phase field parameter (or order parameter) after the transformation stops. From

Fig. 7, it can be seen that the concentration of diffused V_2O_5 in the body of the coating changes from 0.56 (at the reaction surface) to 0 (at a far distance from the reaction surface). Based on the value of the phase equilibrium concentrations previously defined, order parameter of 1 (pure m-phase) is defined at regions with V_2O_5 concentrations greater than or equal to 0.5 (as shown in Fig. 8). While regions with concentration of 0.2 or less contain pure t-phase with order parameter value of 0. Off course, the interfacial region contains mixture of the two phases, and has an order parameter value that range between 0 and 1.

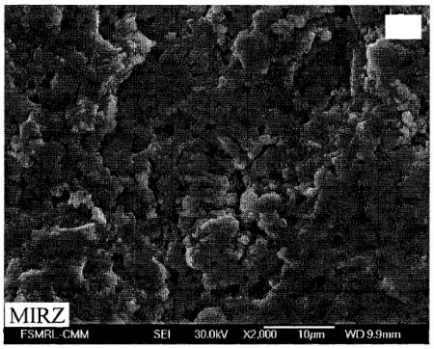

Fig. 6. MIRZ section where lamellar structure is damaged [23].

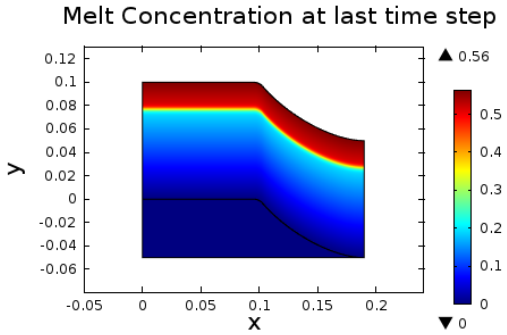

Fig. 7. Concentration of Difffused V_2O_5 after transformation.

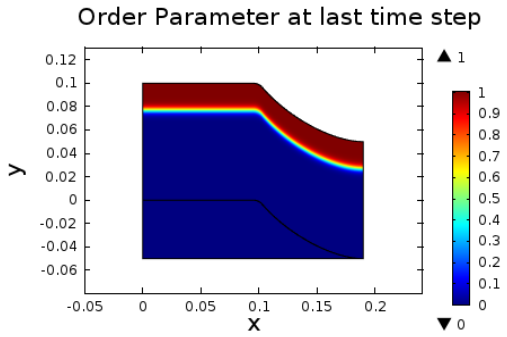

Fig. 8. Order parameter for the evolution of m-phase.

Figure 9 shows the transformation growth of the m-phase. It can be seen that the transformation stops on reaching depth of about 0.0223 μm after approximately 4 milliseconds. It can also be seen that, the transformation exhibits the conventional parabolic growth. This is due to the diffusion of V_2O_5. The small amount of time that is needed for the completion of transformation in the MIRZ conforms to previous experimental findings [4], where it was mentioned that the reaction kinetics in the MIRZ stops in less than 30 minutes. However, the reaction kinetics in the PRZ was shown to continue up to 120 minutes.

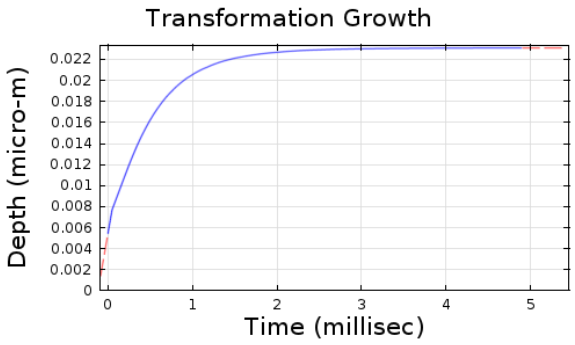

Fig. 9. Transformation depth variation with reaction time.

3.3. Stress analysis

As mentioned previously, the PFM was sequentially-coupled with constitutive model for the prediction of the resulting stress field. The ultimate goal is to predict the nature of the stress field that is developed due to the associated volumetric expansion and the transformation mismatch between the existing phases. This will give insight as to why hot-corroded coatings fail frequently.

Figure 10 shows the strain rate that was extracted from the transformation results and used for the calculation of the 5% volumetric expansion. Figure 11 shows that the 5% volumetric expansion is imposed correctly. There is a strain of 0.02, 0.03 and 0 in the x, y and z directions respectively; thus, giving a total volume expansion of 0.05. The total strain along the thickness of the section is approximately zero, due to the plain strain assumption that was adopted.

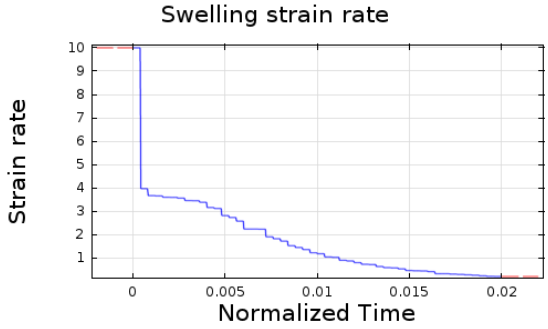

Fig. 10. Variation of volumetric strain rate during transformation.

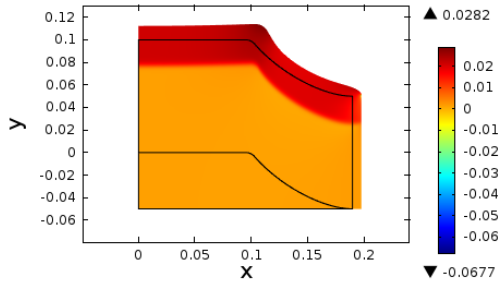

Fig. 11. Volumetric (swelling) strain after transformation.

Figure 12 shows the plot on Von Mises stress field that is developed due to the volumetric expansion of the transformed region and the mismatch in the mechanical properties of the two phases. High stress magnitude of about 1 GPa is observed in some regions, especially at the corners and curvatures that were formed by the micro-cracks. It is also found that, the second and third principal stresses are both compressive, with the first principal stress being zero (shown in Fig. 13). The stresses that are developed in the MIRZ lead to the weakening of the coating, especially near the TGO/bond coat, thus eventually causing the delamination/rumpling of the top coat.

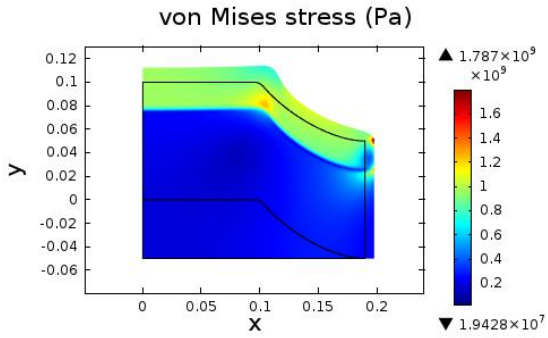

Fig. 12. Von Mises stress after transformation.

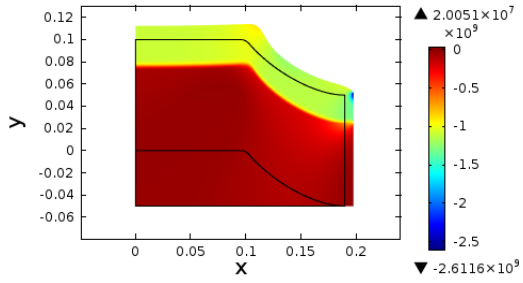

Fig. 13. Third principal stress after transformation.

Figure 14 shows the plot of the Von Mises stress field when the computation is calculated using an enclosed crack. It can be seen that, stresses of very high magnitude are developed due to the closure of cracks which was reported experimentally [4]. The cracks were reported to be closed due to the formation of

reaction products, thus making the reaction kinetics of the MIRZ to stop in less than 30 minutes [4]. Figure 15 shows the variation of the Von Mises stress with time at a selected point in the domain. The stress developed proves to be induced by the transformation, because it also grows according to the reaction kinetics. Cracks with inner curvatures are also found to result in highly stressed corners (that can cause crack-propagation) than those with outer curvatures.

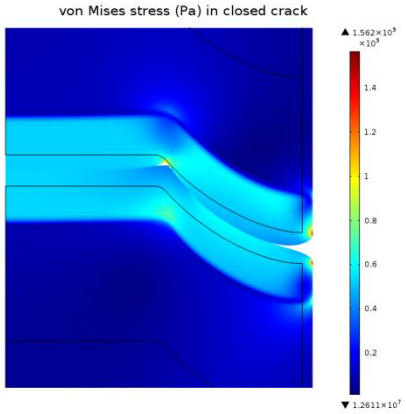

Fig. 14. Von Mises stress after crack closure.

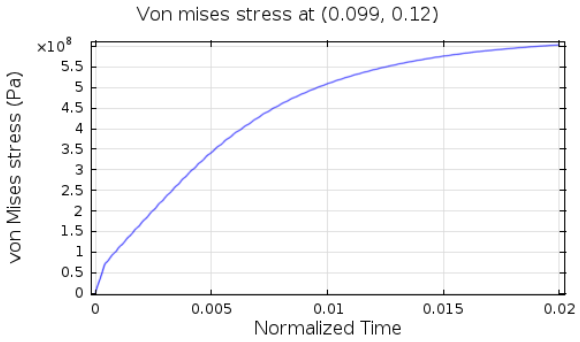

Fig. 15. Variation of Von Mises stress with time.

4. Conclusions

A phase field model that predicts the hot corrosion kinetics in the MIRZ of the top coat was developed. The result obtained shows that, the transformation grows to a thickness of about 0.0223 μm after which the transformation stops. The PFM was sequentially coupled with constitutive model in order to analyse the effect of this transformation on mechanical behaviour of the system.

It was found out that severe internal stresses that lead to the weakening of the material and the propagation of cracks were developed; thus leading to the failure of TBCs. This justifies the previous experimental finding that link the damage of thermal barrier coatings to V_2O_5 melt infiltrations. However, the present study is the first quantitative prediction of the localized stresses formed due to the melt infiltration and the work is mainly numerical. In future work, the experimental prediction of the transformation-induced stresses will be made.

References

1. Padture, N.P.; Gell, M.; and Jordan, E.H. (2002). Thermal barrier coatings for gas turbine applications. *Science Magazine*, 296(5566), 280-284.
2. Perepezko, J.H. (2009). Retrived May, 14, 2014, from https://en.wikipedia. org/ wiki/ Thermal_barrier_coating. Wikipedia.
3. Akhtar, S.S.; Arif, A.F.M.; and Gasem, Z. (2012). Stress field in the top coat of TBC due to the formation of YVO_4-A Numerical Study. *International conference on Surface Modification technologies*, France.
4. Chen, Z.; Mabon, J.; Wen, J.-G.; and Trice, R. (2009). Degradation of plasma-sprayed Yttria-Stabilized Zirconia coatings via ingress of vanadium oxide. *Journal of the European Ceramic Society*, 29(9), 1647-1656.
5. Chen, Z.; Speakman, S.; Howe, J.; Wang, H.; Porter, W.; and Trice, R. (2009). Investigation of reactions between vanadium oxide and plasma-sprayed yttria-stabilized zirconia coatings. *Journal of the European Ceramic Society*, 29(8), 1403-1411.
6. Jones, R.L.; Williams, C.E.; and Jones, A.J. (1986). Reaction of vanadium compounds with ceramic oxides. *Journal of Electrochemical Society*, 133(1), 227-30.
7. Jones, R.L. (1996). Thermal barrier coatings. *Metallurgical and Ceramic Protective Coatings*, Springer Netherlands, 194-235.
8. Mohsen, S.; Abbas, A.; and Akira, K. (2007). Bond coat oxidation and hot corrosion behaviour of APS YSZ coating on Ni super alloy. *Transaction of Joining and Welding Research Institute*, 36(1), 41-45.
9. Hertl, W. (1988). Vanadia reactions with yttria-stabilized zirconia. *Journal of Applied Physics*, 63(11), 5514-5520.
10. Susnitzky, D.W.; Hertl, W.; and Carter, C.B. (1988). Destabilization of zirconia thermal barriers in the presence of V_2O_5. *Journal of Applied Physics*, 71(11), 992-1004.
11. Mecozzi, M.G.; Eiken, J.; Apel, M.; and Sietsma, J. (2011). Quantitative comparison of the phase-transformation kinetics in a sharp-interface and a phase-field model. *Computational Material Science*, 50(6), 1846-1853.
12. Cahn, J.W.; and Hilliard, J.E. (1958). Free energy of a non-uniform system. I. Interfacial free energy. *The Journal of Chemical Physics*, 28(2), 258-267.
13. Allen, S.M.; and Cahn, J.W. (1979). A microscopic theory for anti-phase boundary motion and its application to anti-phase domain coarsening. *Acta Materialia*, 27(6), 1085-1095.
14. Wen, Y.; Chen, L.; and Hawk, J.A. (2012). Phase-field modeling of corrosion kinetics under dual-oxidants. *Modeling and Simulation in Material Science and Engineering*, 20(3), 035013.
15. Tijjani, Y.A.; and Ing. (2008). *Modeling and simulation of thermo-chemical heat treatment processes: A phase field calculation of nitriding in steel*. PhD Dissertation, Bremen University, Germany.
16. Akhtar, S.S.; Abubakar, A.A.; and Arif, A.F.M. (2016). Prediction of residual stresses during gas nitriding of H13 steels using phase field approach. *Journal of Manufacturing Science and Engineering*, 138(1), 011008.

17. Cho, Y.; Kim, J.; Cho, H.; Cha, P.; Suh, D.; Lee, J.K.; and Han, H.N. (2011). Analysis of transformation plasticity in steel using finite element method coupled with phase field model. *PLos ONE*, 7(4), 1-9.
18. Kryvasheyeu, Y. (2012). *The phase field simulation of autocatalytic nucleation*. Thesis. School of Physics, Monash University, Australia.
19. Mamivand, M.; Zaeem, M.A.; Kadiri, H.E.; and Chen, L. (2013). Phase field model of tetragonal-to-monoclinic phase transformation in zirconia. *Acta Materialia*, 61(14), 5223-5235.
20. Abubakar, A.A.; Akhtar, S.S.; and Arif, A.F.M. (2015). Phase field modeling of V_2O_5 hot corrosion kinetics in thermal barrier coatings. *Computational Materials Science*, 99(2015), 105-116.
21. Washburn, E.W. (1921). The dynamics of capillary flow. *Physical Review*, 17(3), 273-283.
22. Pokluda, J.; and Kianicová, M. (2010). Damage and performance assessment of protective coatings on turbine blades, *Gas Turbines*. Gurrappa Injeti (Ed.), ISBN: 978-953-307-146-6.
23. Chen, Z. (2006). *Hot corrosion and high temperature deformation of yttria-stabilized zirconia thermal barrier coatings*. Thesis, Purdue University, West Lafayette, Indiana.
24. Kim, S.G.; Kim, W.T.; and Suzuki, T. (1999). Phase-field model for binary alloys. *Physical Review E*, 60(6), 7186-7196.
25. Vaben, R.; Kerkhoff, G.; and Stover, D. (2001). Development of a micromechanical life prediction model for plasma sprayed thermal barrier coatings. *Material Science and Engineering*: A, 303(1), 100-109.
26. Cao, X.Q.; Vassen, R.; and Stoever, D. (2004). Ceramic materials for thermal barrier coatings. *Journal of the European Ceramic Society*, 24(1), 1-10.
27. Knudsen, J.; Hottel, H.; Sarofim, A.; Wankat, P.; and Knaebel, K. (1997). McGraw-Hill. Ch. Section 5-48: *Heat and Mass Transfer*, Table 5-13.
28. Abubakar, A.A.; Akhtar, S.S.; and Arif, A.F.M. (2013). Phase transformation stress field due to hot corrosion in the top coat of TBC. *International Mechanical Engineering Congress and Exposition (IMECE2013)*, California, USA.
29. Abubakar, A.A.; Akhtar, S.S.; Arif, A.F.M.; and Mostaghimi, J. (2015). The effect of porosity on the hot corrosion failure of thermal barrier coatings. *Modelling and Simulation in Materials Science and Engineering*, 23(7), 075001.